THE AMERICAN SOCIETY OF MECHANICAL ENGINEERS
345 E. 47th St., New York, N.Y. 10017

97-GT-94

PREDICTION OF 3D-UNSTEADY FLOW IN AN AIR TURBINE AND A TRANSONIC COMPRESSOR INCLUDING BLADE GAP FLOW AND BLADE ROW INTERACTION

Alexander R. Jung, Jürgen F. Mayer and Heinz Stetter
Institut für Thermische Strömungsmaschinen und Maschinenlaboratorium
University of Stuttgart
Stuttgart, Germany

ABSTRACT

This paper presents the results of three-dimensional unsteady Navier-Stokes simulations of the flow in a transonic compressor stage with inlet guide vanes and an axial flow air turbine stage with two identical stators for which detailed unsteady experimental data are available. Various unsteady flow phenomena are shown. The focus in the computations are stator/rotor interaction effects. Of special interest are their influences on the flow field downstream of the interface regions. The secondary flow effects are visualized via vector plots. The numerical results are compared with the experimental results. Although there is agood agreement in the major flow phenomena local deviations can be observed.

INTRODUCTION

A significant part of the overall losses in a turbomachine can be attributed to the unsteadiness of the flow, see Dawes (1994). Most contributions to this unsteadiness are caused by the relative motion of subsequent blade rows. The wakes and potential non-uniformities of the upstream blade row interact with the potential of the downstream blade row and are then cut off by the blades. As these pieces of wake travel downstream, they are forced to follow the curvature of the blade-to-blade passage. Simultaneously additional vortices, e.g. passage vortices and tip-clearance vortices, develop as the flow passes by the blade. This already strongly disturbed three-dimensional and highly unsteady flow is getting even more mixed up as it approaches and enters the next blade passage. All these effects add to the losses of the flow. In the process of optimizing the performance of a new blade design it is therefore desirable to include consideration of unsteady effects in order to complement the steady-state studies which are by now the most important possibility to characterize or predict the performance of the new blade. The recent development of more powerful computers especially of affordable high performance workstations and the improved and more efficient numerical methods allow unsteady viscous flow simulations with reasonable spatial and temporal resolutions.

Recently there are lots of projects going on at various research facilities and in industry which are concerned with the analysis of unsteady flow predictions and measurements in turbomachines, see for example Hodson and Dawes (1996), Eulitz et al. (1996), He (1996), Jung et al. (1996), and the contributions to the STS "Turbomachinery" at the *3rd ECCOMAS CFD Conference* (1996). The computations presented in this paper are intended to investigate the capability of a Navier-Stokes solver to predict unsteady flows focusing on stator/rotor interaction and its effects on the downstream flow. The results of the simulation will serve as a base for future projects which will investigate the physics of unsteady losses and their origins in order to develop possibilities to minimize them. The results of flow simulations in a turbine stage with second stator and a transonic compressor stage with inlet guide vane are the examples shown below. The test cases have been chosen since they cover different turbomachine types and since both of these test cases are included in the data base of the *ERCOFTAC Seminar and Workshop on 3D Turbomachinery flow Prediction*, see Gregory-Smith (1993, 1995), and are therefore publicly available.

DESCRIPTION OF THE TEST CASES

Axial Flow Air Turbine

The first application is an axial flow air turbine stage consisting of three blade rows. This test rig is operated at RWTH Aachen where detailed steady-state and unsteady flow field measurements have been carried out, Walraevens and Gallus (1996). The turbine stage consists of two identical stator blade rows and one rotor blade row in between. Geometry data for the turbine is given in Table 1. The setup is quite interesting and challenging with respect to numerical simulations. The flow is subsonic and due to the rather narrow axial gaps between the blade rows (roughly one third of the axial chord length of the stators) and the low aspect ratios of the blades the flow is highly three-dimensional and there are strong secondary flow effects. Furthermore, the rotor tip clearence of 0.7 % of the span adds to the secondary flow effects and needs to be modelled to get reasonable results. In order to take into account the exact ratio of the blade counts without having to discretize the whole machine with all of the 113 blade passages, a method of time-inclination based on the work of Giles (1991) is used as

Presented at the International Gas Turbine & Aeroengine Congress & Exhibition
Orlando, Florida — June 2–June 5, 1997

	stator 1	rotor	stator 2
number of blades	36	41	36
aspect ratio	0.89	0.92	0.89
chord/pitch ratio (mid-span)	1.30	1.44	1.30
blade height	55 mm	55 mm	55 mm
diameter (case)	600 mm	600 mm	600 mm
rotational speed	—	3,500 rpm	—
axial gap (mid-span)	15 mm		15 mm

Table 1: Turbine geometry data

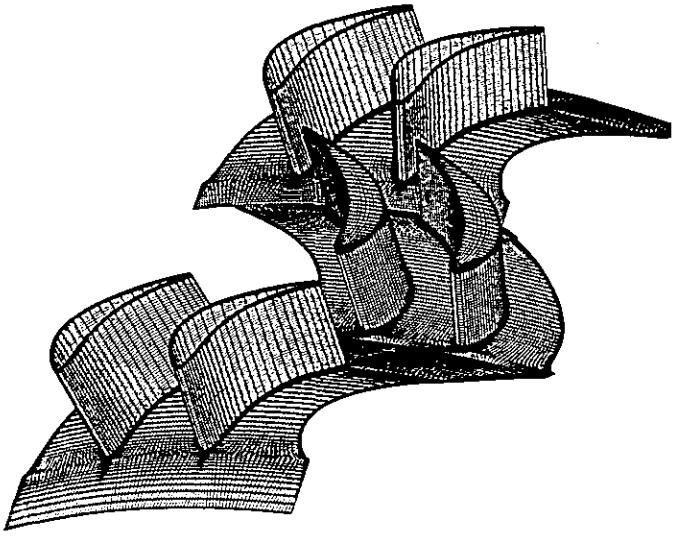

Figure 1: Computational grid for the axial flow air turbine

is described in the section on the numerical method. With this method a single passage calculation can be performed if the difference in the blade counts is not too large. The air turbine stage test case is perfectly suited for this method as the two stator blade rows are identical and the stage pitch ratio of 1.14 lies just within the stability limits of the time-inclination.

Each of the blade rows is discretized with roughly 95,000 nodes making up a total of 287,679 nodes for the computational domain including the rotor tip gap which is discretized with 4,275 nodes. A three-dimensional view of the computational mesh on the hub, on the blade surfaces and on the rotor blade tip is depicted in Fig. 1. In the narrow rotor hub region the axial length of the passage is only slightly larger than the axial chord length of the blade. Therefore, the short inflow and outflow channels of the rotor domain are modelled with only 5 grid lines in axial direction such that the stator/rotor interfaces are very close to the rotor blades leading and trailing edges respectively. Due to the rather thick rotor blades which have a modified VKI profile, the blade gap is modelled with 19 grid lines in circumferential direction. Thus, the tip gap grid generation deserves due attention, especially near the leading and trailing edge where there are high gradients of the mesh size.

Transonic Compressor Stage with IGV

The second test case presented is a transonic compressor stage with inlet guide vane for which steady-state experimental data was obtained at Ecole Centrale de Lyon. Each of the three blade rows consists of

	IGV	rotor	stator
number of blades	33	57	58
aspect ratio	1.5	1.5	1.2
chord/pitch ratio (hub)	0.98	1.67	1.72
chord/pitch ratio (case)	0.76	1.18	1.39
blade height (mid-chord)	60 mm	57 mm	49 mm
diameter (case)	550 mm	544 mm	534 mm
rotational speed	—	11,500 rpm	—
axial gap (hub)	41 mm		41 mm
axial gap (case)	45 mm		46 mm

Table 2: Compressor geometry data

a different number of blades and the largest common denominator of the blade counts is equal to 1, see Table 2. Therefore each of the IGV flow channels has a different position with respect to the flow channels of the second stator. The time-inclination method can only be applied to more than one stator/rotor interface if all pitch ratios are identical or an integer multiple of each other. Thus, an unsteady simulation of this compressor configuration without simplifying assumptions would require to model the whole machine including all of the 148 blades and to analyse the flow field for the whole annulus during one blade passing period in order to ensure that all possible variations of the rotor position relative to each blade of the IGV and the stator are captured. Even with todays high performance computers a reasonably discretized three-dimensional Navier-Stokes simulation of this problem including the necessary post-processing of the data coming along with it is hardly possible.

Thus, a different approach is followed here in order to perform a simulation with acceptable memory and CPU time requirements: only the flow in the two downstream blade rows is simulated with the unsteady method whereas a steady-state interaction of the flow with the upstream IGV blade row is realized by coupling circumferentially averaged flow variables in a non-reflective manner at the corresponding interface region. For implementation details about the different interface treatments see Jung et al. (1996) for the unsteady method and Merz et al. (1995) for the steady-state method. Combining steady-state coupling and direct unsteady coupling in a single calculation allows to easily calculate the unsteady flow in each of the stages of a turbomachine without having to care about inter-blade row boundary conditions as they evolve naturally from the computation itself. Knowledge of boundary conditions is only necessary for the very first inlet and the last exit boundary. Furthermore, with this approach it is also possible to simulate the unsteady flow in multiple stages with arbitrary pitch ratios simultaneously as long as there is at least one steady-state interface in between two stages if the pitch ratios of these stages are not integer multiples of each other. The results of such a "partial" unsteady simulation and a "real" unsteady calculation are somewhat different, of course, since the direct unsteady interaction between two stages is not modelled in this approach and e.g. the influence of remainders of upstream flow non-uniformities is averaged out by the steady-state coupling. However, due to the modelling of the unsteadiness in single stages and the implementation of the coupling method, the circumferentially averaged flow variables that are used to model the steady-state interaction are comparable to time-averaged quantities and are therefore closer to steady-state measurements, than this is the case if these boundary conditions are extracted from a pure steady-state simulation where unsteady effects are not modelled at all.

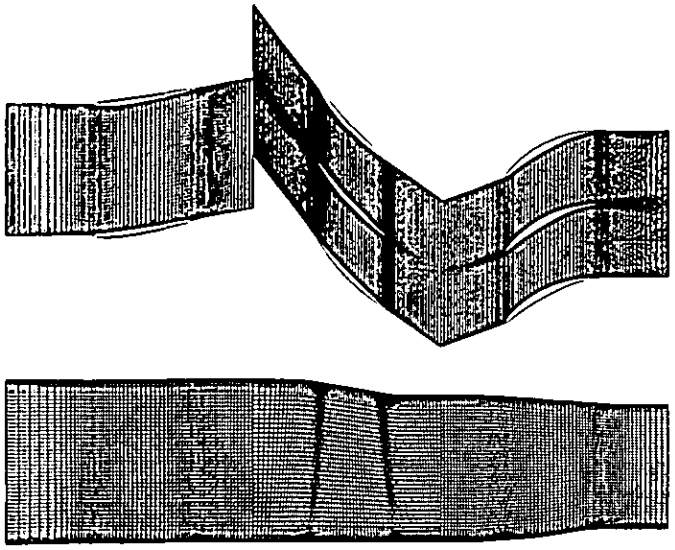

Figure 2: Computational grid for the transonic compressor (top: azimuthal cut at mid-span, bottom: meridional cut)

The calculation presented below uses the circumferentially averaged coupling at the interface between the IGV and the rotor, whereas direct unsteady interaction is simulated for the rotor and the downstream stator blade row. The flow in the domain of the IGV is expected to be steady and is not simulated with the time-accurate methodd. Therefore all acceleration techniques applicable to steady-state simulations (e.g. local time-stepping, full multi-grid, residual smoothing) can be used for this domain. The other possibility, where the unsteady IGV/rotor interaction is simulated while at the rotor/stator interface circumferentially averaged flow variables are coupled will be investigated in the next future.

The stage pitch ratio resulting from 57 rotor blades and 58 stator blades does not lead to any problems with the time inclination method. A special challenge to the numerical method, however, are the very narrow radial blade gaps. In this compressor test case each blade has such a gap as none of the blade rows is shrouded. The conical blade gap of the stator blade poses a special difficulty because of the zero gap width at the trailing edge. This cannot be handled with a structured grid solver and a tiny gap has to be modelled. Each blade passage is disretized with about 250,000 nodes yielding a total of 747,261 nodes for the computational domain. The computational grid for the machine at mid-span is shown on the top of Fig. 2. The plot at the bottom of this figure depicts a meridional cut through the computational domain.

NUMERICAL METHOD

The equations solved are the fully three-dimensional, unsteady, Favre-averaged Navier-Stokes equations. The set of equations is written for a cylindrical coordinate system that rotates at constant angular velocity, see Jung et al. (1996). The fluid is assumed to behave as an ideal gas with a constant ratio of specific heat capacities. A modified algebraic Baldwin-Lomax model is used to describe the effects of turbulence.

The governing equations are discretized in space in finite volume form on curved hexahedral control volumes. The state variables are located at the vertices of each cell and a piecewise linear variation over the cell faces between the vertices is assumed. The method to evaluate the convective and diffusive residuals of each control volume and to add artificial diffusion in order to prevent odd-even decoupling and to control shock capturing is of a standard Jameson type, see Jameson et al. (1981). The net flux imbalance for each control volume is used to update the flow variables through a five-stage Runge-Kutta time stepping scheme which is modified according to Jameson.

In cases of unsteady simulations in which the stator blade count is different from the rotor blade count, a time-inclining method for three dimensions based on the work of Giles (1991) is used in order to model the exact ratio of the blade counts. In this approach, time-transformations are applied to both the stator and the rotor domains and different time steps are used in these domains. In this way simple periodicity conditions can be applied at the boundaries in pitch-wise direction although these boundaries are not periodic in the physical domain.

At the inlet and exit boundaries as well as at boundaries between two domains in the case of steady-state flow interaction of two blade rows, a non-reflecting post-correction method based on the work of Giles (1988) is applied to prevent spurious reflections from waves that leave the computational domain. Solid surfaces are assumed adiabatic and the no-slip condition is applied. Periodicity in pitch-wise direction is ensured through the use of dummy cells that keep copies of the periodic values such that the points on these boundaries can be treated like interior points.

Block-structured H-type grids which consist of curved hexahedral cells and which are fixed in the relative frame of reference are used in a multi-block topology in order to allow easy modelling of blade gaps as well as of computational domains which consist of multiple blade passages. At the sliding interfaces between stationary and rotating blade rows the grids are overlapped by one grid cell. An interpolation procedure consistent with the second order spatial accuracy of the numerical scheme is used to interchange the flow variables during every time step of the intergration procedure. As the rotor grid moves relative to the stator, the rotation of the rotor is integrated in time in order to track the position of the grid blocks for a time-resolved coupling at the interface regions.

For steady-state calculations a full multi-grid method as well as implicit residual smoothing with variable coefficients can be used to accelerate convergence to a very large extent, see Merz et al. (1995). In the case of unsteady calculations a time-consistent multigrid scheme based on the work of He (1996) and an implicit residual averaging method for global time steps may be used to accelerate the solution process.

RESULTS

Axial Flow Air Turbine

A steady-state simulation was carried out in order to get the initial data for the unsteady calculation. Due to the small cells in the tip gap region 2,000 time steps per blade passing period were required in the unsteady calculation. The time-consistent multi-grid method was chosen as the only acceleration technique. In this way the error introduced by accelerating the simulation can be better estimated than with residual averaging. The latter may influence the solution in a wider part of the domain due to the implicit formulation than this is the case for the multi-grid method, see He (1996). The efficiency of the accelerated

Figure 3: Instantaneous entropy contours at mid-span at time $t = 0$

calculation was about 10 times higher than that of the unaccelerated scheme. Each time step took about 12 seconds on a single processor of a NEC SX-4. The experimentally obtained mass flow rate of 6.71 kg/s is in good agreement with that of the simulation which amounts to 6.73 kg/s.

Instantaneous entropy contours in an azimuthal cut at mid-span are shown in Fig. 3. Due to the unequal pitches of the rotor and the stator, the flow in each of the depicted passages can be viewed as the flow in a single passage but at different instants in time. From this diagram it can be observed how the wake of the first stator enters the rotor passage until it is eventually cut off by the rotor blade. The remainders of the stator wakes are then convected downstream and dissipate to a certain extent before they enter the passage of the second stator together with the rotor wakes. Caused by this process, a highly unsteady flow develops. Due to the low aspect ratio blades, this flow is dominated by strong secondary flow effects and passage vortices at the hub and the casing, tip leakage vortex, trailing edge vortex and remainders of the upstream stator exit flow non-uniformities characterize the highly unsteady flow. These effects can be visualized e.g. in cross-flow sections in and downstream of the rotor passage by means of secondary velocity vectors plots. Presently, the analysis of the results is still in progress in order to extract all interesting information from the data. Especially for unsteady flows, comparison with measurement data is quite extensive with respect to the number of plots required to do so. Due to space limitations only some examples of the results are shown. The vector plots in Fig. 5 depict instantaneous secondary flow fields in the absolute frame of reference in the axial gap between the rotor and the second stator. The results are shown in comparison with the measurement data for eight different instants in time during one blade passing period. The numerical results are on the left side of each pair of plots whereas the experimental results are depicted on the right. In the measurements, the upper and lower radial position of the probe is 5 mm away from the hub and the casing respectively. The measurements cover an angle of 12 degrees in circumferential direction, which is 20 % wider than the stator pitch. The results of the simulation are therefore shown for two stator pitches. The window which is outlined by a dotted line in the plots of the computational results shows the approximate position of the corresponding domain of interest in the experiments. When comparing the results it should be kept in mind that the direction of the secondary flow vector may differ slightly as the different sizes of the cutting planes may lead to different average flow angles. Note also that the experimental and computational results are not synchronized exactly but there might be a maximal offset of 3 % of the stator blade pitch due to different definitions in the point of reference. However, in spite of all of these considerations, it can be stated, that even with these preliminary results, the major vortex systems identified in the experiments can be found in the computational results as well, although there are some discrepancies in the absolute location of the vortex cores as well as in the strength of the vortices. The corresponding relative Mach number distribution is shown in the contour plots of Fig. 7. The double minima in the center of the rotor wake are captured reasonably well and may be used as a starting point for the comparison. The experimental data indicate a more dissipated wake with less steep gradients than the numerical results. This might be due to turbulence modelling and the treatment of the wake. The good agreement in the locations of the single peak at about 70 % of span at time $t = 0.625T$ might be accidental, but is nonetheless interesting to note.

The instantaneous secondary flow field in the passage of the second stator near the trailing edge during a blade passing period is depicted in Fig. 9. It can be observed from these diagrams how the formation of the stator hub and casing passage vortices is strongly disturbed by the periodically occuring remainders of the rotor exit flow non-uniformities.

Transonic Compressor Stage with IGV

In order to get an initial solution for the flow field, a steady-state calculation was performed. Similar to other simulations of this test case, see e.g. Gregory-Smith (1993), it was not possible to reach the nominal mass flow rate with the nominal pressure rise of the compressor of 1.36. The simulation showed regions of separated flow in the rotor and the stator domain. Rather large separation bubbles were convected downstream causing the mass flow rate to oscillate significantly with the frequency of the appearance of the bubbles which was about half an order of magnitude lower than the blade passing frequency. The measurements did not indicate this type of flow behaviour. The simulated effect could be due to the discretization being too coarse and thus yielding a simulation which is too dissipative and which may produce some sort of numerical stall in the compressor, especially as the high nominal pressure ratio is close to surge conditions. Although the turbulence model allows flow separations, the predicted size of those might not be very physical. Besides, the different time scales of the separation bubbles and the stator/rotor interaction effects would make the analysis of the flow field much more complicated.

Therefore the stator exit pressure was decreased, what caused not only the mass flow rate to increase to about the nonimal rate but also the flow to reattach almost completely. Thus, the results shown below are for a computation with the stator outlet pressure being reduced by about 8 %. The time step size was 1/1000 of the blade passing period and each time step took about 36 seconds of CPU time on a single

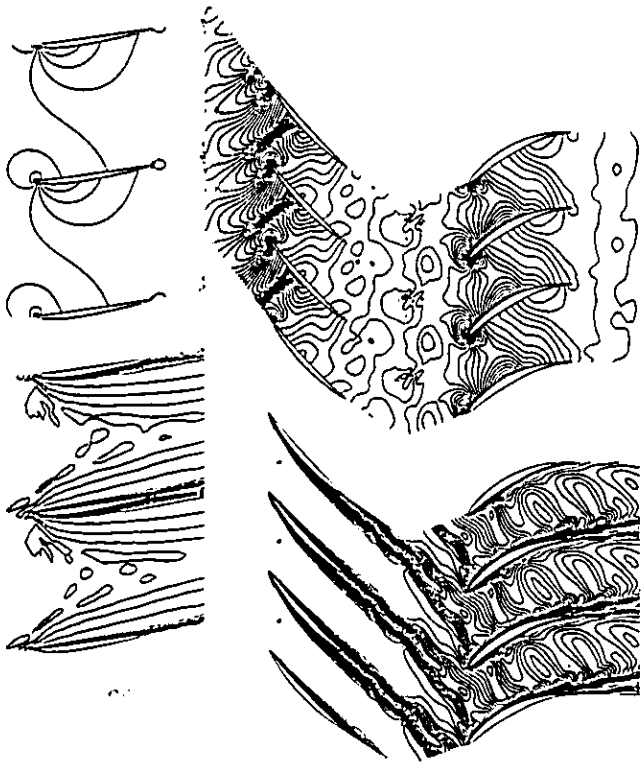

Figure 4: Instantaneous static pressure (top) and entropy (bottom) contours at mid-span at time $t = 0$

processor of a NEC SX-4.

Azimuthal views of the instantaneous flow field at mid-span at time $t = 0$ are depicted in Figs. 4. These diagrams show contour lines of the static pressure and entropy distribution in the compressor. The different interface treatments between the IGV and the rotor on one hand and between the rotor and the stator on the other hand is quite obvious. Other interesting features in the plots are the shock in the rotor passage and the rotor wakes which are cut off by the stator blades and then convected downstream through the stator passage.

Further examples of the numerical results for the compressor are shown in Figs. 8, 6, and 10. A sequence of contour plots depicting the instantaneous entropy distribution in a meridional cut through the middle of the passage in the stator domain at five instants in time during one blade passing period is shown in Fig. 10. In these plots it can be observed how the rotor wake enters the stator domain and travels downstream where it mixes out to a certain extent and gets disturbed by other flow phenomena. Interesting in this sequence is the strongly disturbed flow near the casing which is caused by a separation bubble from the rotor tip region that was entering the domain of interest during the previous period.

The instantaneous entropy distribution at the stator exit is shown in Fig. 6. In this time sequence it can be observed how the vortex systems which have developed during the flow past the stator passage mix up the remainders of the rotor wakes even more before they finally leave the domain. The dominant hub passage vortex rolls upward along the stator and dissolves itself finally at about 70 % of the span when the next vortex already starts developing near the hub. This unsteady flow behaviour is also illustrated in Fig. 8 by means of vector plots of the secondary flow field at the same location.

CONCLUSIONS

The capability of a Navier-Stokes solver to simulate the three-dimensional unsteady flow in different types of turbomachines is investigated. The computational results of the flow for two test cases are presented. Examples of the various unsteady flow phenomena that can be identified in these machines are shown. The flow through the 1.5-stage air turbine features strong secondary flow effects and complex vortex systems. Comparison with experimental results is made and reasonable agreement in the major flow features can be stated. However, there are discrepancies for some local flow effects and their locations. In the transonic compressor stage with IGV and radial gaps on each blade tip, strong secondary flow and stator/rotor interaction effects are identified and illustrated.

The experience with these preliminary results will be the base for further studies in order to investigate mechanisms of unsteady loss production in turbomachines. Further computations with finer meshes will be used for more detailed comparison of available unsteady experimental data and the predicted flow fields. Improving the knowledge on unsteady flow physics and the loss production mechanisms in turbomachines will finally help to develop methods for designing more efficient blades.

REFERENCES

Dawes, W. N., 1994, "A Numerical Study of the Interaction of a Transonic Compressor Rotor Overtip Leakage Vortex with the Following Stator Blade Row," ASME 94-GT-156.

Eulitz, F., Engel, K., Gebing, H., 1996,"Numerical Investigation of the Clocking Effects in a Multistage Turbine," ASME 96-GT-026.

Giles, M. B., 1988, "Non-Reflecting Boundary Conditions for the Euler Equations," Tech. Rep. TR-88-1, MIT CFD Laboratory.

Giles, M. B., 1991, "UNSFLO: A Numerical Method for the Calculation of Unsteady Flow in Turbomachinery," GTL Rep. No. 205, MIT Gas Turbine Laboratory.

Gregory-Smith, D. G., 1993, "The ERCOFTAC Seminar and Workshop on 3D Turbomachinery Flow Predictions – December 1992", ASME 93-GT-423.

Gregory-Smith, D. G., 1995, "3D Flow Simulation in Turbomachinery – The ERCOFTAC Seminar and Workshop III, January 1994", VDI-Berichte 1185, pp. 35–49.

He, L., 1996, "Time-Marching Calculations of Unsteady Flows, Blade Row Interaction and Flutter", VKI-LS 1996-05.

Hodson, H. P., Dawes, W. N., 1996, "On the Interpretation of Measured Profile Losses in Unsteady Wake-Turbine Blade Interaction Studies," ASME 96-GT-494.

Jameson, A., Schmidt, W., Turkel, E., 1981, "Numerical Solutions of the Euler Equations by Finite Volume Methods Using Runge Kutta Time-Stepping Schemes," AIAA 81-1259.

Jung, A. R., Mayer, J. F., Stetter, H., 1996, "Simulation of 3D-Unsteady Stator/Rotor Interaction in Turbomachinery Stages of Arbitrary Pitch Ratio", ASME Paper 96-GT-69.

Merz, R., Krückels, J., Mayer, J. F., Stetter, H., 1995, "Calculation of Three-Dimensional Viscous Transonic Turbine Stage Flow Including Tip Clearance Effects", ASME Paper 95-GT-76.

Special Technological Session: Turbomachinery, 1996, Third ECCOMAS Computational Fluid Dynamics Conference, Sept. 9–13, 1996, Paris, France.

Walraevens, R. E., Gallus, H. E., 1996, "Stator-Rotor-Stator Interaction in an Axial Flow Turbine and its Influence on Loss Mechanisms", AGARD-CP-571, 39/1–39/14.

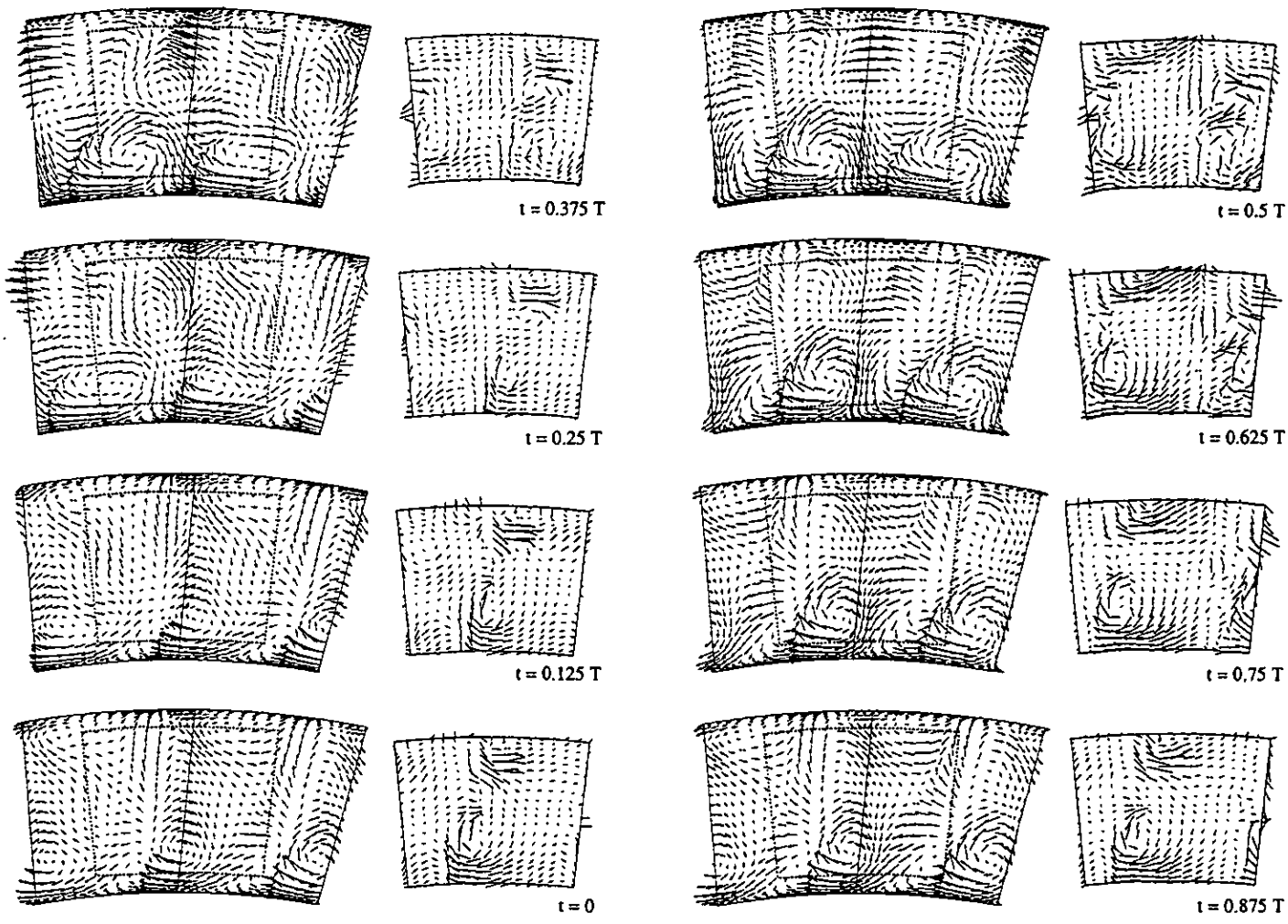

Figure 5: Instantaneous secondary flow field at the rotor exit in the absolute frame during a blade passing period T (left: simulation, right: experiment)

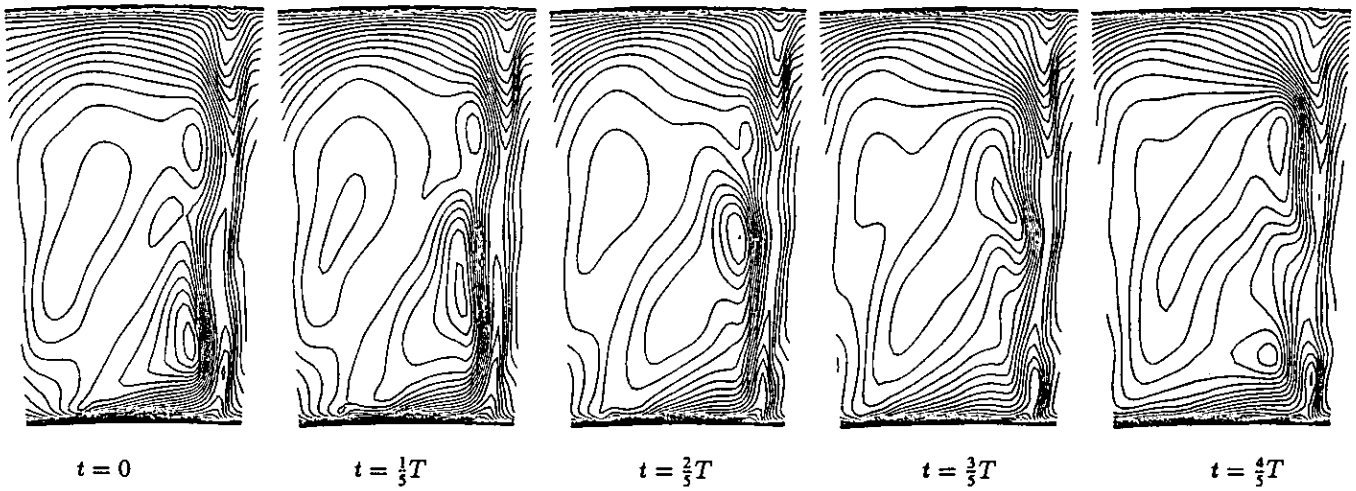

Figure 6: Instantaneous entropy distribution at the exit of the stator during a blade passing period T

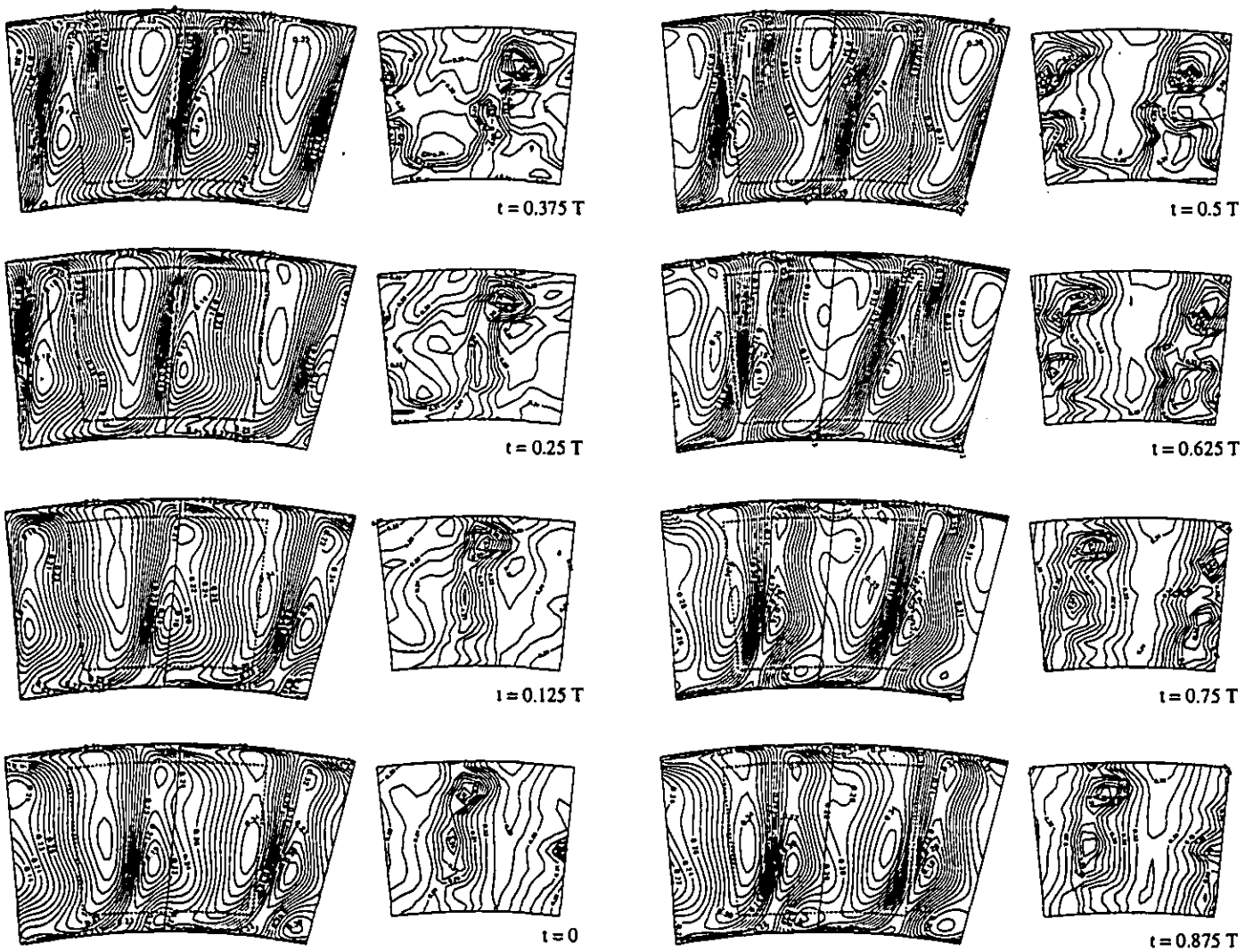

Figure 7: Instantaneous relative Mach number distribution at the rotor exit during a blade passing period T (left: simulation, right: experiment)

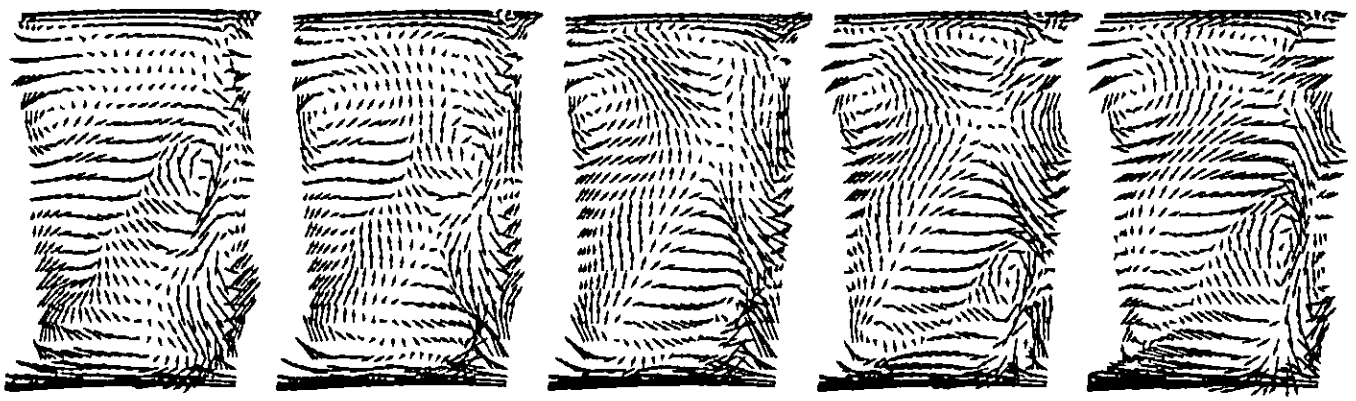

Figure 8: Secondary flow field at the exit of the stator during a blade passing period T

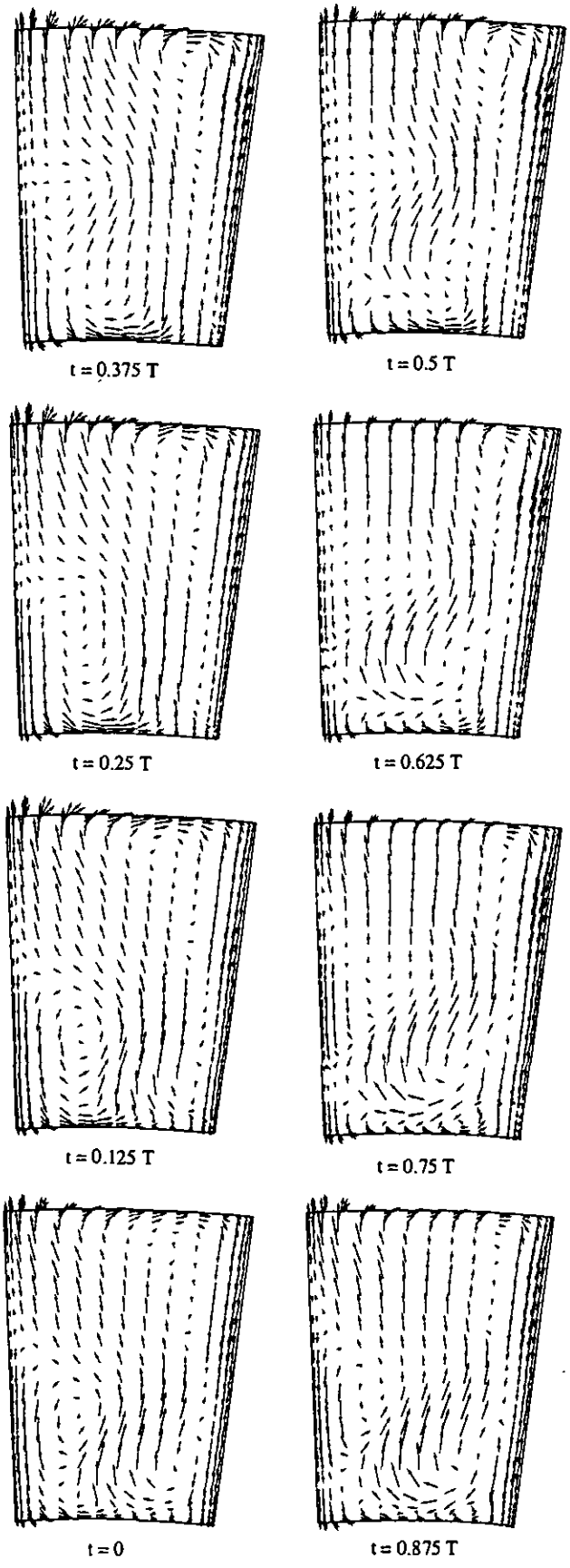

Figure 9: Instantaneous secondary flow field in the passage of the second stator near the trailing edge during a blade passing period T

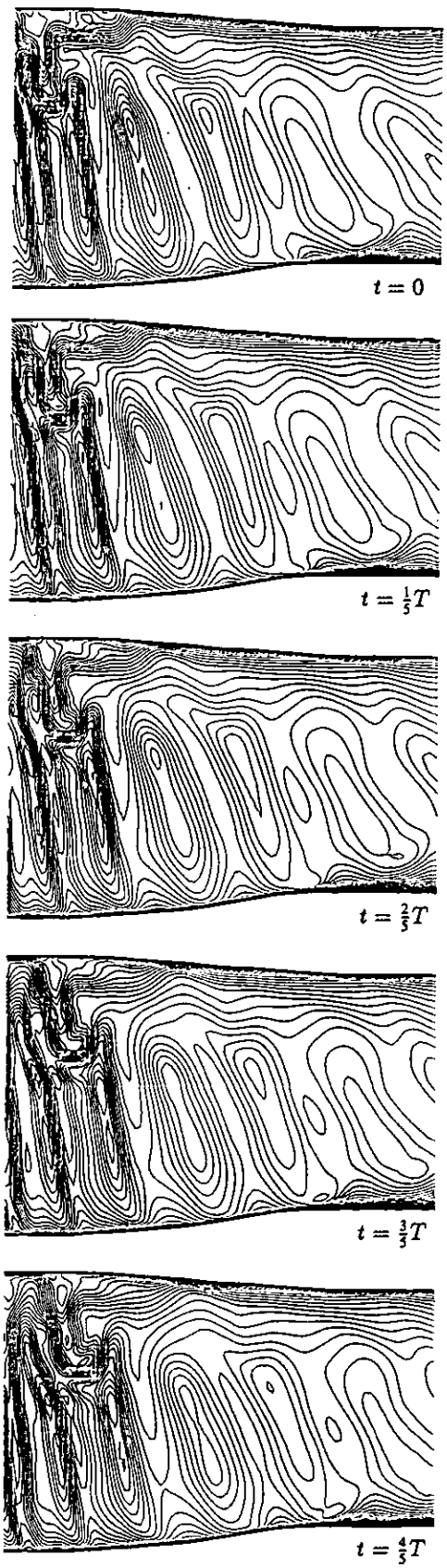

Figure 10: Instantaneous entropy distribution in a meridional cutting plane through the middle of the stator passage during a blade passing period T